Hindawi Publishing Corporation
Shock and Vibration
Volume 2014, Article ID 436156, 10 pages
http://dx.doi.org/10.1155/2014/436156

Research Article

Development of a Numerical Model for an Expanding Tube with Linear Explosive Using AUTODYN

Mijin Choi,[1,2] Jung-Ryul Lee,[1,2,3] and Cheol-Won Kong[4]

[1] *Department of Aerospace Engineering, Chonbuk National University, 567 Baeje-daero, Deokjin-gu, Jeonju 561-756, Republic of Korea*
[2] *LANL-CBNU Engineering Institute Korea, Chonbuk National University, 567 Baeje-daero, Deokjin-gu, Jeonju 561-756, Republic of Korea*
[3] *Department of Mechatronics Engineering, Chonbuk National University, 567 Baeje-daero, Deokjin-gu, Jeonju 561-756, Republic of Korea*
[4] *Structures and Material Department, Korea Aerospace Research Institute, Daejeon 305-333, Republic of Korea*

Correspondence should be addressed to Jung-Ryul Lee; leejrr@jbnu.ac.kr

Received 24 October 2012; Accepted 14 March 2013; Published 24 March 2014

Academic Editor: Gyuhae Park

Pyrotechnic devices have been employed in satellite launch vehicle missions, generally for the separation of structural subsystems such as stage and satellite separation. Expanding tubes are linear explosives enclosed by an oval steel tube and have been widely used for pyrotechnic joint separation systems. A numerical model is proposed for the prediction of the proper load of an expanding tube using a nonlinear dynamic analysis code, AUTODYN 2D and 3D. To compute a proper core load, numerical models of the open-ended steel tube and mild detonating tube encasing a high explosive were developed and compared with experimental results. 2D and 3D computational results showed good correlation with ballistic test results. The model will provide more flexibility in expanding tube design, leading to economic benefits in the overall expanding tube development procedure.

1. Introduction

Pyrotechnic devices are widely used in many space applications. They are used to perform releasing, cutting, pressurization, ignition, switching, and other mechanical work to initiate flight sequences during space missions, such as the separation of subsystems, boosters, fairings, stages, or payload satellites. Such explosive separation devices generate a shock environment that could have a destructive effect on the structure and hardware, especially on electromechanical and optical equipment. The environment is very complex, and studies have revealed that little information is available describing the basic mechanism of shock transmission and predicting shock response. Therefore, improved guidelines for pyrotechnic design, development, and qualification are clearly needed [1–3].

Pyrotechnic devices may generally be divided into point sources and line sources. Typical point sources include explosive bolts, separation nuts, pin pullers and pushers, and certain combinations of point sources for low explosive actuation. Typical linear sources include flexible linearly shaped charges, mild detonating fuses, and Super∗Zip for high explosive actuation [4, 5].

An example of line sources is shown in Figure 1. The pyrotechnic device shown is a high-load-carrying separation system that must act without contamination of the payload and is called an expanding tube in this study. The device is one of the greatest shock producers in aerospace separation systems. The detailed components of the expanding tube are also represented in Figure 1, consisting of an MDF (mild detonating fuse), support, and a flattened steel tube. The MDF is a small diameter extruded tube containing a single strand of explosive cord. It is manufactured by filling a tube with explosive material and extruding the tube using a conventional, multiple-die, cold extrusion process [6–9]. Structure separation is accomplished when the MDF is ignited. When an MDF is initiated, the detonation is propagated along

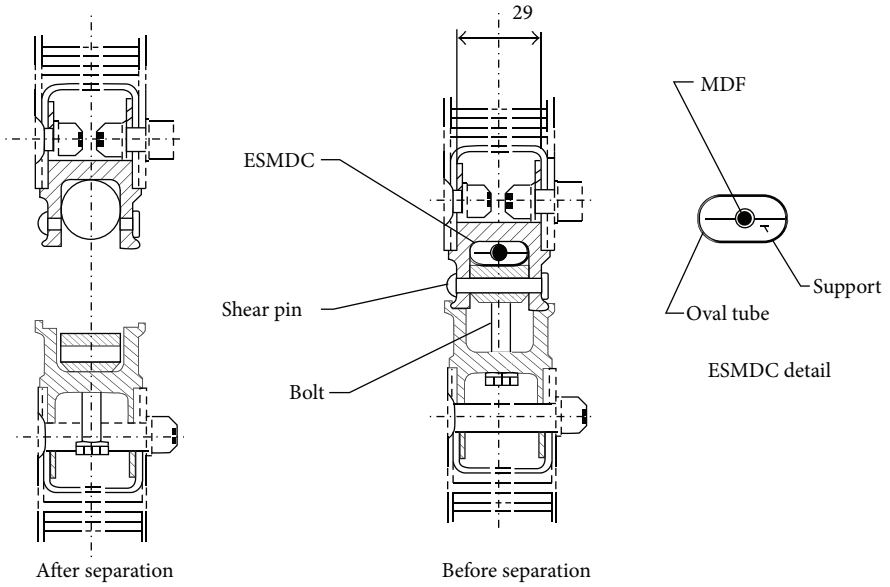

Figure 1: A pyro-separation system [9].

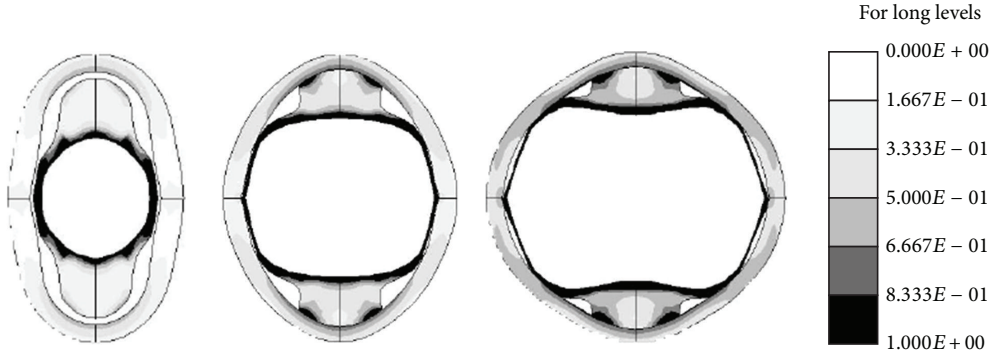

Figure 2: Numerical simulation of expanding tube free expansion [10].

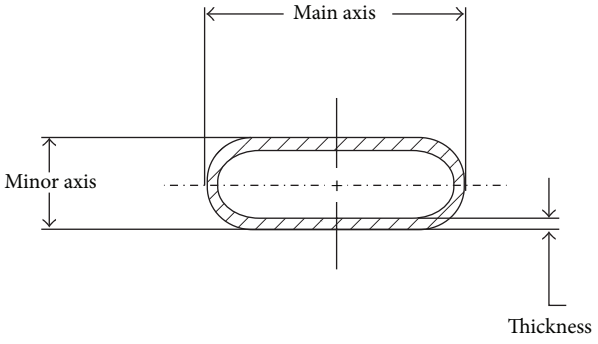

Figure 3: Geometry of expanding tube.

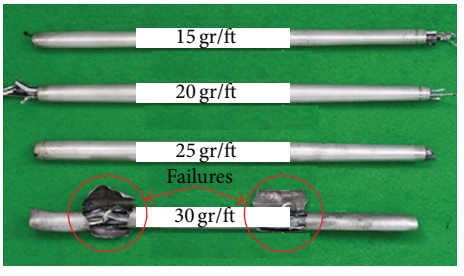

Figure 4: Experimental results of expanding tube.

the entire length of the linear explosive at a VOD (velocity of detonation) between 6.0 and 7.5 km/s, with very high shock energy. This chemical reaction acts as mechanical loading, which allows the elliptical steel tube to expand mainly in the minor-axis direction and fractures pin joints. Consequently, the expanded tube can separate structures according to its design, without contamination [8]. Since the performance of expanding tubes is mainly related to the explosive load, investigation of the proper explosive load against expanding tube failure and structural damage is important to its design.

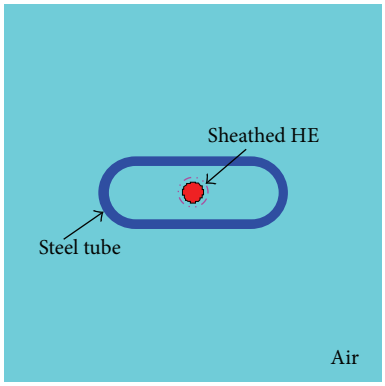

Figure 5: Material location of two-dimensional expanding tube.

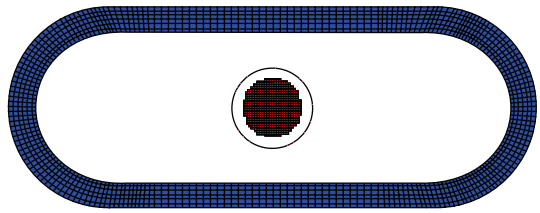

Figure 6: Two-dimensional expanding tube numerical model.

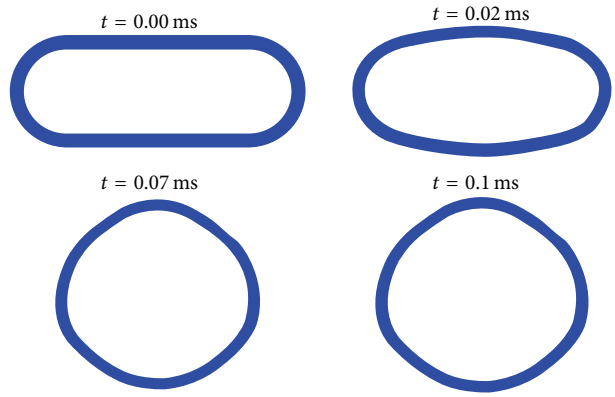

Figure 7: Expanding tube distortions (explosive load 15 gr/ft).

Even if the expanding tube design has to be verified in ballistic tests, adding a numerical simulation step between the expanding tube sample fabrication and its ballistic test can be a more effective approach for proper explosive load determination. The numerical model can explain the full physics of the phenomena by solving the governing equations that describe the behavior of the system under consideration.

In spite of the advantages of numerical simulation, only a few numerical and experimental investigations on pyrotechnic devices can be found in the literature. Quidot [10] adopted LSDYNA to simulate a pyrotechnic separation system. A line source comprised an expanding tube with a 1 mm thick stainless steel case, internal synthetic material, and a lead-RDX cord with a 2 g/m RDX charge. Numerical simulations were performed for this device, as shown in Figure 2. However, the proper explosive load, which is the most important factor for real-world applications of expanding tube design, was not addressed under consideration of the detonation wave propagation, the fracture mechanism, and experimental validation.

In this study, two- and three-dimensional numerical analyses of expanding tube were performed in order to develop a numerical model with high accuracy. The explicit dynamic code AUTODYN is adopted to simulate expansion of the tube and compute a proper core load. AUTODYN is a hydrocode program that is especially suited to solve the interaction problems of different systems of structure, liquid, and gas together, as found in many studies of high explosive simulation [11–15]. To verify the accuracy of the developed model, the numerical results were compared to experimental ballistic test results for different explosive load conditions.

2. Ballistic Tests of Expanding Tubes

Experiments were performed to properly design a pyrotechnic device. Explosive tests were carried out for different core loads of 15, 20, 25, and 30 gr/ft. The expanding tube is an open-ended cylinder, in which an MDF filled with hexanitrostilbene (HNS) explosive is set along the central axis of the cylinder. All MDF cords were manufactured with 3 mm diameters regardless of the respective explosive loads, and the wall thickness of the sheath was 0.1 mm. Figure 3 represents a section view of an expanding tube with a major axis of 20 mm, a minor axis of 8 mm, and a thickness of 1 mm, regardless of the core load. The tests were carried out 4 or 5 times for each core case, and the deformed shape and failure were investigated. Figure 4 shows the results of ballistic tests with explosive core loads of 15, 20, 25, and 30 gr/ft. Expanding tubes with 15, 20, and 25 gr/ft were freely expanded without failure. In contrast, the 30 gr/ft expanding tube failed at both ends of the cylinder, as shown in Figure 4. The dimensions of each expanding tube were measured, and these measurements were averaged. These results are used to validate the numerical model, which will be discussed in Section 3.

It can be deduced from the ballistic test results that the threshold explosive load of the tested samples must lie between 25 gr/ft and 30 gr/ft. Ballistic tests are a good approach to determine a proper explosive load for expanding tubes, as well as a better approximation of actual conditions. However, this experimental approach has several disadvantages, in which ballistic tests typically require many expanding tube samples and connected structures, which are also damaged during the test and are nonreusable. The experimental method is also not flexible for design change and is expensive and time consuming. Moreover, it is difficult to explain the physical phenomena of structure and detonation interactions. Therefore, to mitigate this problem, the ballistic test should be the final confirmation test of the expanding tube development procedure, after replacing the numerous case samples with a reliable numerical model.

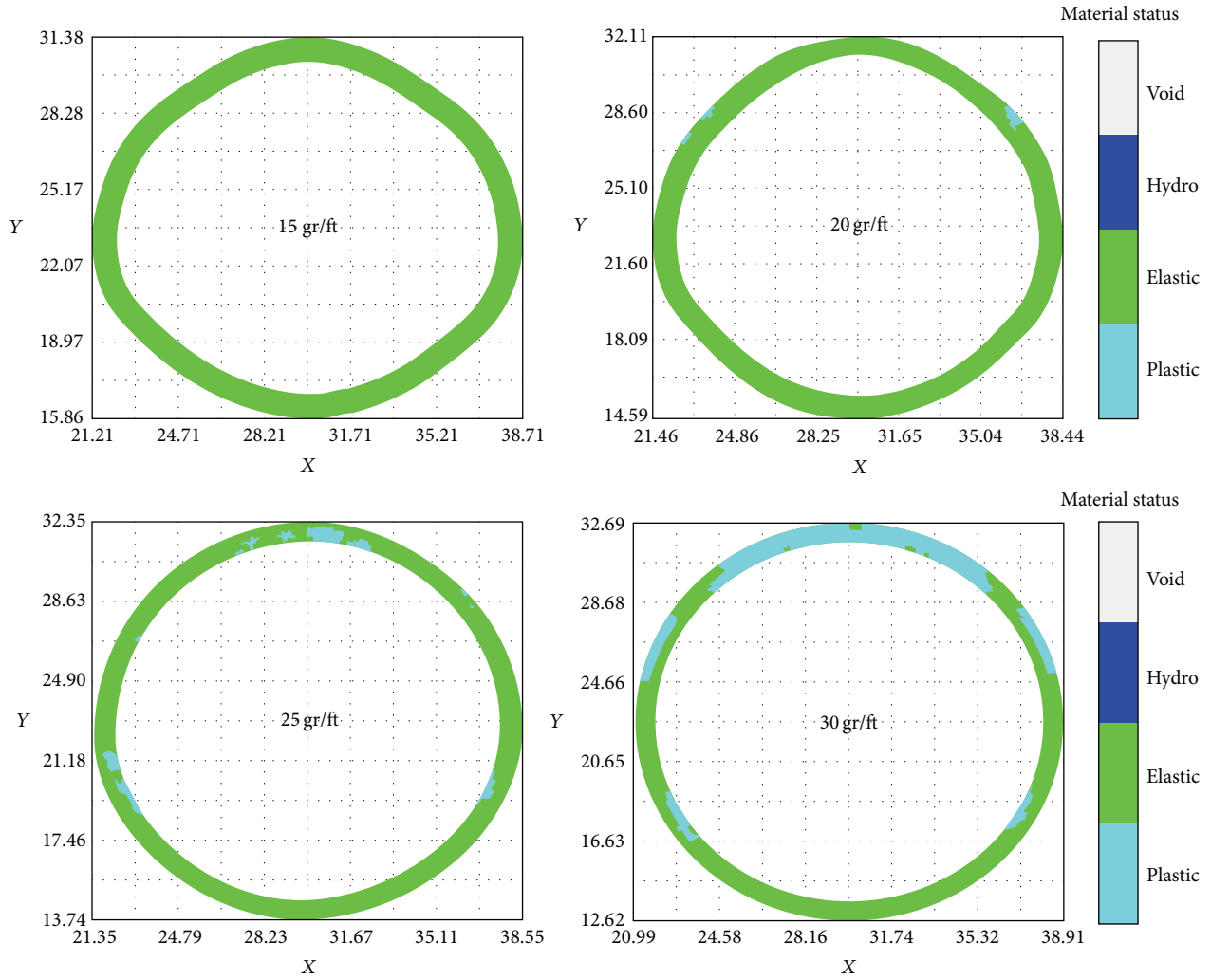

Figure 8: Material status of expanded steel tube.

3. Numerical Modeling

3.1. Numerical Model. Numerical simulations were performed for all the experiments using hydrocode in AUTODYN 2D, examining the experimental expanding behavior and numerical stresses. The two-dimensional model was made of a steel tube, support, MDF, and surrounding air, as shown in Figure 5. The surrounding air was modeled as an ideal gas, and the area was 400 mm × 400 mm. Since the material of the support layer was Teflon and it did not affect tube expansion significantly, it was assumed as air. The explosive material was HNS 1.65, where 1.65 indicates the density of HNS which is 1.65 g/cm^3. The explosive loads for all cases ranged from 15 to 30 gr/ft. The explosive propagation velocity for HNS 1.65 was approximately 7,030 m/s, and the detonation point was set to the center of the MDF.

3.2. Material Description and Boundary Conditions. Both the reacted solid and reacted gaseous products of HNS 1.65 explosive were characterized with the Jones-Wilkins-Lee

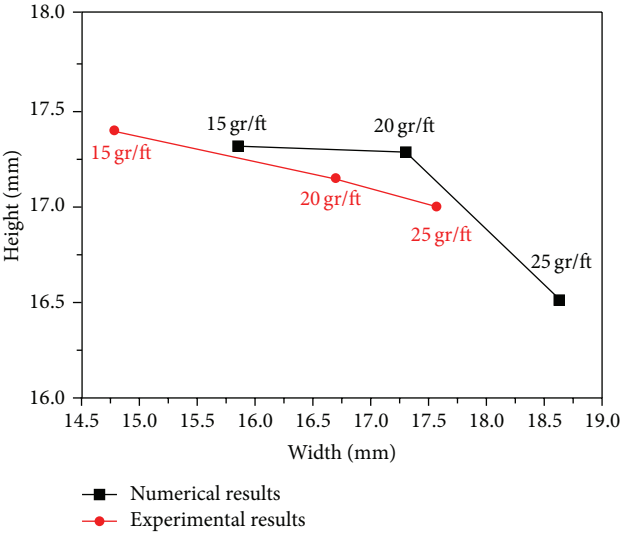

Figure 9: Comparison between the experimental and calculational results.

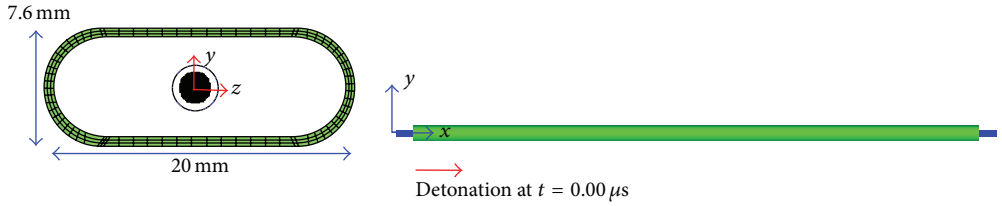

Figure 10: Three-dimensional expanding tube.

Table 1: Material coefficients in Jones-Wilkins-Lee (JWL) equation for HNS 1.65.

Parameter	Value	Unit
A	4.65×10^8	kPa
B	8.87×10^6	kPa
R_1	4.55	—
R_2	1.35	—
ω	0.35	—

equation of state (JWL EOS, [16]). The pressure in either phase is defined in terms of volume and internal energy independent of temperature as

$$p = A\left(1 - \frac{\omega}{R_1 V}\right)e^{-R_1 V} + B\left(1 - \frac{\omega}{R_2 V}\right)e^{-R_2 V} + \frac{\omega e}{V}, \quad (1)$$

where $V = \rho/\rho_o$ is the relative volume, e is the internal energy, and A, B, R_1, R_2, and ω are empirically determined constants that depend on the kind of the explosive. Table 1 lists the JWL EOS coefficients used for this analysis of the HNS with a density of 1.65 g/cm^3.

The ideal gas EOS for air is shown as follows:

$$p = (\gamma - 1)\rho e, \quad (2)$$

where γ is the ideal gas constant and ρ and e are the density and internal energy of the air. The internal energy of air at room temperature and ambient pressure is 2.068×10^5 kJ.

Both the tube and sheath were modeled as SS304 steel and AL6061. With the high pressure resulting from explosive detonation, both the tube and sheath undergoing high strain rates were modeled using the shock equation of state [17] and Steinberg-Guinan strength model [18]. Both the von Mises yield strength (Y) and the shear modulus (G) of the Steinberg-Guinan model are assumed to be described as a function of pressure (P), density (ρ), and temperature (T), and, in the case of yield strength, the effective plastic strain as well (ε):

$$G = G_0\left(1 + \left(\frac{G_0'}{G_0}\right)\frac{p}{\eta^{1/3}} + \left(\frac{G_T'}{G_0}\right)(T - 300)\right),$$

$$Y = Y_0\{1 + \beta(\varepsilon + \varepsilon_i)\}^n \quad (3)$$

$$\times\left(1 + \left(\frac{Y_p'}{Y_0}\right)\frac{p}{\eta^{1/3}} + \left(\frac{Y_T'}{Y_0}\right)(T - 300)\right),$$

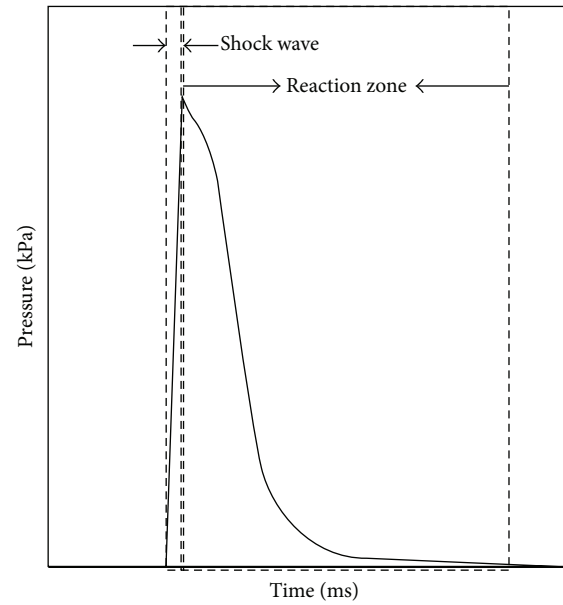

Figure 11: Pressure loading profile.

where β is the hardening constant and n is the hardening exponent. The subscript 0 refers to the reference state (T = 300 K, P = 0, ε = 0). The primed parameters with the subscripts P and T indicate the derivatives of the parameters with respect to pressure or temperature at the reference state. Table 2 summarizes the Steinberg-Guinan strength parameters used for the numerical model for the SS304 steel and AL6061 used in the present analysis.

A flow-out condition was applied to all boundaries of the Euler grid. This allowed the material to freely leave the grid and also prevented relief waves from being generated off the lateral boundaries of the solid, which would reduce the overall strength of the compressive shock and rarefaction waves.

3.3. Failure Model. Spallation (spall-fracture) is a kind of fracture that occurs as planar separation of material parallel to the incident plane wave fronts as a result of dynamic tensile stress components perpendicular to this plane [19]. The spall strength for tensile stress generated when a rarefaction wave travels through material is 2.1 GPa for the steel tube. If the tensile stress of the tube exceeds the predefined spall strength,

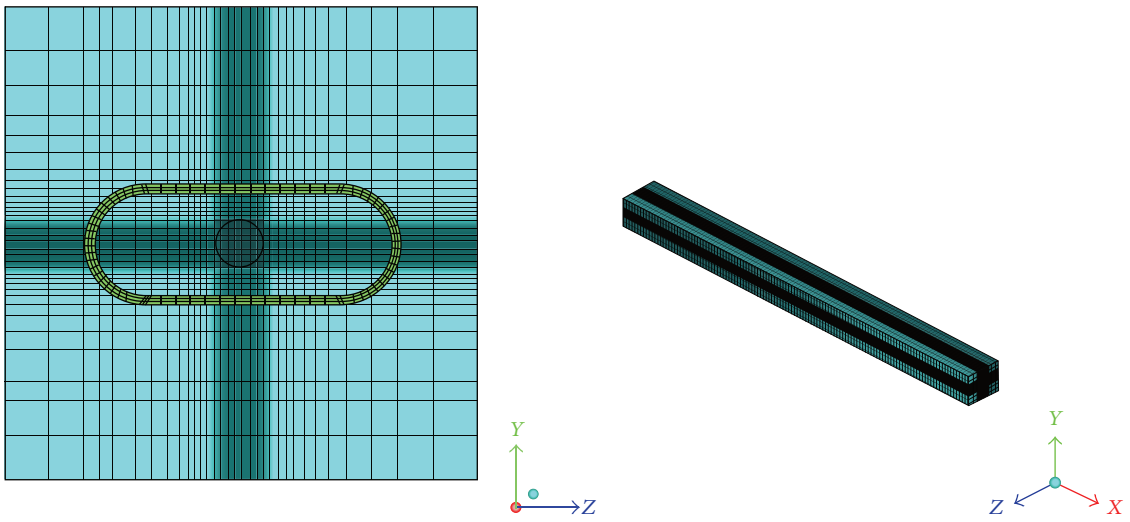

(a) (b)

Figure 12: Three-dimensional model of expanding tube (front view (a) and isotropic view (b)).

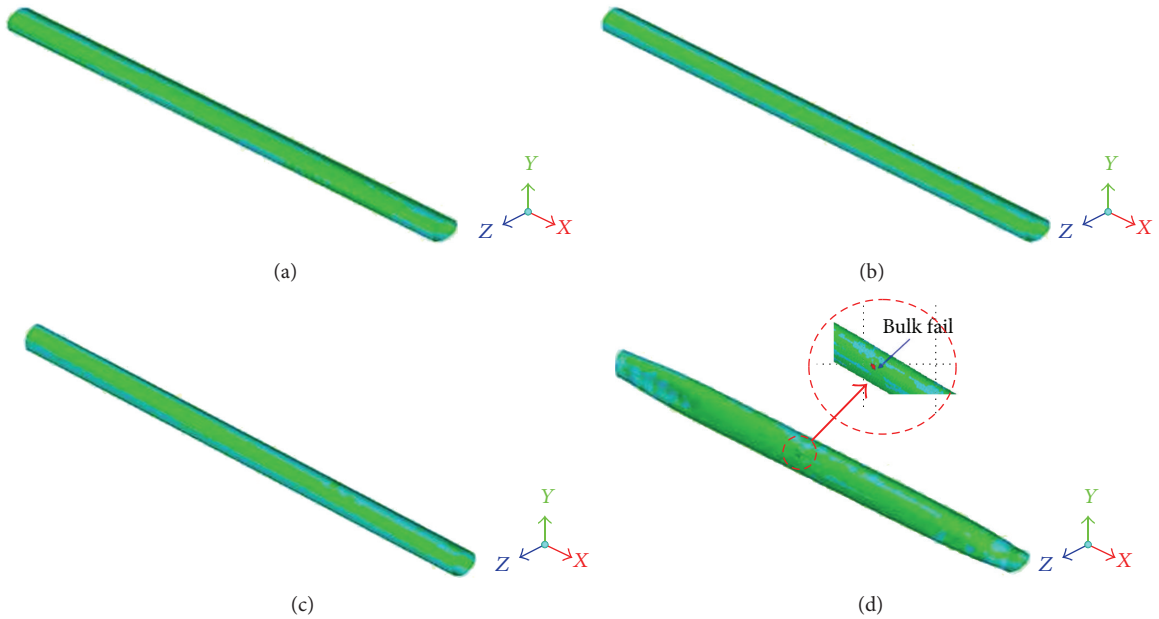

(a) (b) (c) (d)

Figure 13: Material status of one-sided detonation expanding tube ((a): 15 gr/ft, (b): 20 gr/ft, (c): 25 gr/ft, and (d): 30 gr/ft).

the material is considered to have "failed." The tensile stress produced by a rarefaction wave is often shown as a negative pressure [14].

3.4. Solvers. AUTODYN provides various solvers for nonlinear problems [11, 20, 21]. Lagrange and Euler solvers were adopted in these FSI (fluid-structure interaction) simulations. The Lagrangian representation keeps material in its initial element, and the numerical mesh moves and deforms with the material. The Lagrange method is most appropriate for the description of solid-like structures. Eulerian representation allows materials to flow from cell to cell, while the mesh is spatially fixed. The Eulerian method is typically well suited for representing fluids and gases [20–23]. In this study, the steel tube and sheath were modeled using a Lagrange solver, while HNS and air were modeled using an Euler solver. The Euler and Lagrange interaction was also implemented to take into account the interaction between fluid (explosive and air) and structures (tube and sheath). This coupling technique allows complex fluid-structure interaction problems that

Table 2: Steinberg-Guinan strength parameters.

Parameter	SS304	AL6061	Unit
G	7.7×10^8	2.97×10^7	kPa
Y	3.4×10^5	5×10^4	kPa
β	43	28	—
n	0.35	0.8	—
dG/dP	1.74	1.4	
dG/dT	-3.5×10^4	-1.29×10^4	kPa/K
dY/dP	7.68×10^{-3}	2.35×10^{-3}	—
Melting temperature	2380	1604	K

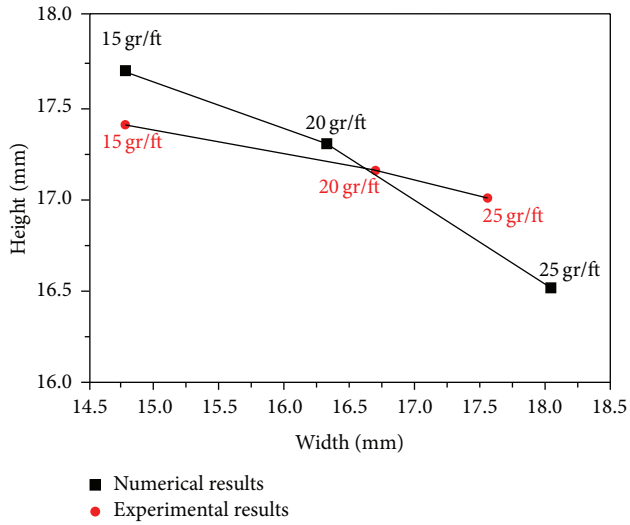

Figure 14: Comparison between the experimental and calculational results.

include large deformation of the structure to be solved in a single numerical analysis.

4. Results and Discussion

4.1. Two-Dimensional Numerical Results. Figure 6 shows the two-dimensional numerical model of an expanding tube explosion. The cell width was approximately 0.16 mm. The number of elements in the tube model was 1,404, and the whole model had 161,504 elements. A description of the numerical model is shown in Table 3.

To illustrate the expansion process of the steel tube over time, the deformed configurations of a 15 gr/ft expanding tube are depicted in Figure 7 at $t = 0$ ms, 0.02 ms, 0.07 ms, and 0.1 ms. The calculation was started at time $t = 0.0$ ms and finished at $t = 0.1$ ms, when it could be assumed that detonation had been completed. It is clearly seen that the tube is expanded outward radially from the detonation point. At $t = 0.02$ ms, early in the detonation, the minor axis of the tube started to be expanded, and the length of the major axis was becoming shorter over time. At a later time, the shape of the tube section was deformed from elliptical to circular, such that the shape change might separate a joint.

Table 3: Description of numerical model of 2D expanding tube.

Part	Materials	Number of mesh	Solver
Tube	SS304	1,404	Lagrangian
Sheath	AL6061	100	
Air	Air	160,000	Eulerian
High explosive	HNS 1.65		

A series of computations was performed by varying explosive loads to compute the material response of the tube, and the deformations are presented in Figure 8. It is apparent that the tube expansion increases as the explosive load increases. For a pressure tube in the plastic deformation regime, catastrophic failure is associated with ductile tearing or plastic instability [19, 24, 25]. Rapidly expanding regions (the minor axis of the tube) are accompanied by rapid loss of stress-carrying capability and intense heating due to the dissipation of plastic work, and present risks of rupture [26]. As shown in Figure 8, the plastic region and computed stress were increased proportionally to the explosive load. As a result, the 30 gr/ft expanding tube shows the largest plastic region, and the greatest stress is on the minor axis due to energy absorption. However, the 30 gr/ft expanding tube expanded without spallation in the 2D simulation, which differs distinctly from the experimental results, because this FE analysis accounts for only radial expansion. This suggests that the tube expansion due to the detonation wave propagation should be considered to develop a more reliable numerical model.

Figure 9 compares the changes of width and height of the tube in the FE analysis and experimental results for three cases, with 15, 20, and 25 gr/ft. Although the calculation results slightly overestimated the experimental results of each core load, the overall error of both width (minor axis) and height (major axis) prediction was less than 10%.

4.2. Three-Dimensional Numerical Results. Figure 10 illustrates a three-dimensional expanding tube and detonation direction. The open-ended steel tube was 300 mm long, and MDF of a 320 mm length of MDF was inserted into the central bore. Its cross section was the same as in the 2D case. Detonation was assumed to be started from the left end of the tube at $t = 0.0$ ms, identically to the experimental conditions. To describe the 3D detonation propagation, a cylindrical blast wave was generated and then remapped in the air. The pressure profile of the detonation wave propagation into the tube is presented in Figure 11, and its structure consists of a shock wave and reaction zone, where the explosive is changed into gaseous products at high temperature. These reaction products act as a piston that allows the shock wave to propagate at a constant velocity [27]. Figure 12 shows the numerical model of the 3D expanding tube. A graded grid was applied to the air and HNS 1.65 to save computation time. Table 4 summarizes the description of the 3D numerical model.

Figure 13 displays the expansion behaviors and material status of each expanding tube. Similar to the 2D results,

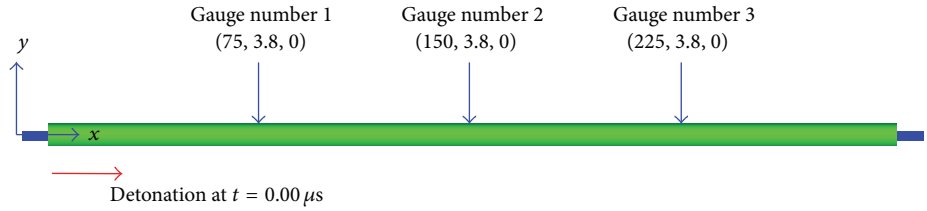

Figure 15: Gauges position.

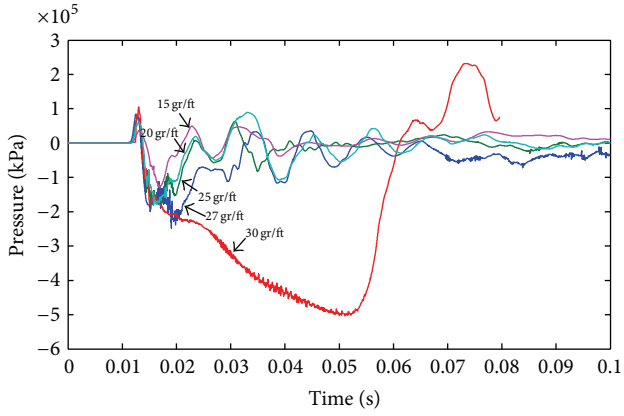

Figure 16: Pressure histories from gauge number 1.

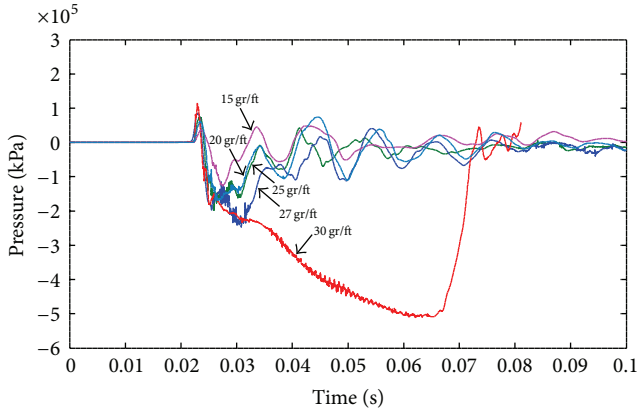

Figure 17: Pressure histories from gauge number 2.

Table 4: Description of 3D expanding tube numerical model.

Part	Materials	Number of mesh	Solver
Tube	SS304	64,800	Lagrangian
Sheath	AL6061	13,360	
Air	Air	203,125	Eulerian
High explosive	HNS 1.65		

the tubes with explosive loads of 15–25 gr/ft freely expanded, but the 30 gr/ft tube failed due to plastic deformation. As shown in Figure 13, there was spallation at 130 mm from the side of the 30 gr/ft expanding tube at around $t = 0.07$ ms. This ductile fracture was caused by the significant amount

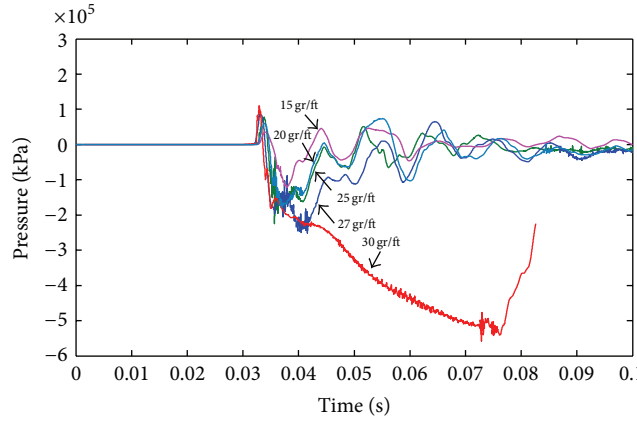

Figure 18: Pressure histories from gauge number 3.

of plastic deformation during tube expansion. This failure behavior in FE analysis was somewhat different from the experimental failure behavior. In experiments, two failures occurred on the left and right sides of the steel tube, while one bulk failure was found in the numerical simulation. Even if the first spallation could be predicted, it might be inappropriate to simulate a successive multiple-spallation generation mechanism.

Figure 14 compares between the numerical simulation and experimental results of each expanding tube deformation. The overall error was less than 3%, and the agreement was improved by considering the tube expansion due to detonation wave propagation.

To compute a proper core load, the internal pressure of the expanding wall of the steel tube was numerically calculated for explosive loads of 15, 20, 25, 27, and 30 gr/ft. The three points indicated in Figure 15 represent the placement of a gauge for measuring the internal pressure. Figures 16, 17, and 18 plot the time histories of pressure observed by gauges in the middle of the steel tube thickness over time. The first peak was due to the initial shock wave traveling through the tube. The rarefaction wave generated due to free surface interaction is often shown as negative pressure following the first peak, and it produces tensile stress on the tube. The maximum pressure of the respective gauges ranged from −130 to −520 MPa for the various explosive loads. The pressure histories of expanding tubes with loads of 15–25 gr/ft fluctuated and became stable over time. In the FE analysis, the 27 gr/ft expanding tube was able to expand freely without failure, and its maximum pressure was

1.25 times higher than that of the 25 gr/ft expanding tube, which was found to have a proper explosive load in the ballistic test using expanding tube samples. Therefore, we can conclude that the proper explosive load in the experiments was underestimated according to the numerical results. For an explosive load of 30 gr/ft, the internal pressure increased dramatically and reached a value of −520 MPa. The maximum pressure on the steel tube with the 30 gr/ft load was about 2.7 and 2 times higher than those with the 25 gr/ft and 27 gr/ft loads, respectively. This means that, since the explosive load of 30 gr/ft was greater than the failure threshold, spallation occurred in the actual expanding tube.

5. Conclusions

The development of a numerical model has been presented for the free expansion of expanding tubes by MDF detonation in pyro-separation systems using AUTODYN 2D and 3D hydrocode. Numerical simulations were performed for four expanding tube explosive load cases as a verification set for the numerical model, and additional simulation was done to suggest a more effective explosive load.

In the 2D model, since the detonation wave propagation could not be considered, the results slightly overestimated the shape of the expanded tube. To improve the accuracy of the results, the 3D model was developed, which allowed for tube expansion due to detonation wave propagation. The developed model was verified with explosive test results and showed less than 3% overall error. From the results of 3D numerical simulation, where the Steinberg model was applied for the failure criteria of the steel tube, 27 gr/ft was the proper explosive load, and the 30 gr/ft explosive load exceeded the threshold of expanding tube failure. Since the numerical model verified with ballistic test results allows for various design changes, the development cost and time can be greatly reduced by minimizing the number of experimental tests required. Therefore, it is suggested to add a numerical model development step using 3D hydrocode to the overall procedure of expanding tube development for pyrotechnic separation systems.

Conflict of Interests

The authors declare that there is no conflict of interests regarding the publication of this paper.

Acknowledgments

This research was supported by the Leading Foreign Research Institute Recruitment Program (2011-0030065) and the Basic Science Research Program (2011-0010489) through the National Research Foundation of Korea, funded by the Ministry of Education, Science, and Technology. This study was also financially supported by the University Collaboration Enhancement Project of the Korea Aerospace Research Institute.

References

[1] K. Y. Chang and D. L. Kern, Super∗Zip (linear separation) shock characteristics, 1986, http://ntrs.nasa.gov/archive/nasa/casi.ntrs.nasa.gov/19870011172_1987011172.pdf.

[2] L. J. Bement and M. L. Schimmel, "A manual for pyrotechnic design, development and qualification," NASA Technical Memerandum 110172, 1995.

[3] J. R. Lee, C. C. Chia, and C. W. Kong, "Review of pyroshock wave measurement and simulation for space systems," *Measurement: Journal of the International Measurement Confederation*, vol. 45, no. 4, pp. 631–642, 2012.

[4] K. Y. Chang, "Pyrotechnic devices, shock levels, and their applications," in *Proceedings of the Pyroshock Seminar, ICSV9*, 2002.

[5] NASA, "Pyroshock test criteria," NASA-STD-7003A, 2011.

[6] L. H. Richards, J. K. Vision, and D. J. Schorr, "Thrusting separation system," US Patent, US5372071, 1993.

[7] W. C. Hoffman III, "Age life evaluation of space shuttle crew escape system pyrotechnic components loaded with hexanitrostilbene (HNS), NASA," Technical Paper 3650, 1996.

[8] L. J. Bement and M. L. Schimmel, "Investigation of Super∗Zip separation joint," NASA Technical Memorandum 4031, 1988.

[9] M. Miyazawa and Y. Fukushima, "Development status of Japan's new launch vehicle: H-II rocekt," in *Proceedings of the 40th Congress of the International Astronautical Federation*, 1989.

[10] M. Quidot, "Some examples of energetic material modeling with LSDYNA," in *Proceedings of the 3rd European LS-DYNA Conference*, 2001.

[11] G. E. Fairlie, "The numerical simulation of high explosives using AUTODYN-2D & 3D," in *Proceedings of the Institute of Explosive Engineers 4th Biannual Symposium (Explo '98)*, 1998.

[12] J. K. Chen, H. Ching, and F. A. Allahdadi, "Shock-induced detonation of high explosives by high velocity impact," *Journal of Mechanics of Materials and Structures*, vol. 2, no. 9, pp. 1701–1721, 2007.

[13] S. M. Muramatsu, "Numerical and experimental study of a pyroshock test set up for small spacecraft component," Project Report, UPNA, 2010.

[14] J. Danyluk, *Spall fracture of multi-material plates under explosive loading [M.S. thesis]*, Rensselaser Polytechnic Institute at Hartford, Hartford, Conn, USA, 2010.

[15] R. H. B. Bouma, A. E. D. M. van der Heijden, T. D. Sewell, and D. L. Thompson, "Chapter2. Simulations of deformation processes in energetic materials," in *Numerical Simulations of Physical and Engineering Processes*, 2011.

[16] E. L. Lee, H. C. Hornig, and J. W. Kury, "Adiabatic expansion of high explosive detonation products," Technical Report UCRL-50422, Lawrence Radiation Laboratory, University of California Livermore, Berkeley, Calif, USA, 1968.

[17] M. A. Meyers, *Dynamic Behavior of Materials*, Wiley, New York, NY, USA, 1994.

[18] D. J. Steinberg, S. G. Cochran, and M. W. Guinan, "A constitutive model for metals applicable at high-strain rate," *Journal of Applied Physics*, vol. 51, no. 3, pp. 1498–1504, 1980.

[19] J. N. Johnson, "Dynamic fracture and spallation in ductile solids," *Journal of Applied Physics*, vol. 52, no. 4, pp. 2812–2825, 1981.

[20] ANSYS, *Workshop 7. Ship Blast, ANSYS Training Manual*, ANSYS, Cecil Township, Pa, USA, 2010.

[21] ANSYS, *Chapter 1. Introduction to AUTODYN, AUTODYN Training Manual*, ANSYS, Cecil Township, Pa, USA, 2010.

[22] X. Quan, N. K. Birnbaum, M. S. Cowler, B. I. Gerber, R. A. Clegg, and C. J. Hayhurst, "Numerical simulation of structural deformation under shock and impact loads using a coupled multi-solver approach," in *Proceedings of the 5th Asia-Pacific Conference on Shock and Impact Loads on Structures*, 2003.

[23] Century Dynamics, *AUTODYN Theory Manual*, Century Dynamics, Concord, Calif, USA, 2003.

[24] J. E. Shepherd, "Structural response of piping to internal gas detonation," *Journal of Pressure Vessel Technology, Transactions of the ASME*, vol. 131, no. 3, pp. 0312041–03120413, 2009.

[25] J. Kanesky, J. Damazo, K. Chow-Yee, A. Rusinek, and J. E. Shepherd, "Plastic deformation due to reflected detonation," *International Journal of Solids and Structures*, vol. 50, no. 1, pp. 97–110, 2013.

[26] A. J. Rosakis and G. Ravichandran, "Dynamic failure mechanics," *International Journal of Solids and Structures*, vol. 37, no. 1-2, pp. 331–348, 2000.

[27] S. Fordham, *High Explosives and Propellants*, Pergamon Press, Elmsford, NY, USA, 2nd edition, 1980.